Finite Difference Simulation of Interacting Resonance and Pulse Waves in a Nonlinear Material

by

© **Matthew Williams**

A thesis submitted to the Department of Physics and Physical Oceanography in partial fulfillment of the requirements for the degree of B.Sc.(Hons).

Department of Physics and Physical Oceanography
Department of Mathematics and Statistics

Memorial University

May 2021

St. John's, Newfoundland and Labrador, Canada

Abstract

The field of nonlinear acousto-elastic behaviour in materials such as rocks is an area of active research, applicable to phenomena such as earthquakes or material fatigue. This nonlinearity arises from the rock microstructure, notably through cracks, and appears in the form of a nonlinear relation between the stress and strain fields within the rock. We study how this nonlinearity manifests when the sample is in either a resonant or a transient state. To do this, we numerically model a sample including a crack and broadcast a low frequency pump wave and a high frequency probe wave through the sample. We use a fourth order finite difference scheme to model the evolution of wave velocity, stress, and strain, then use a form of averaging to represent the cracked, heterogeneous model with an effective homogeneous model. Calculating the nonlinear interactions between the two waves allows us to compare the resonant and transient behaviour. We demonstrate differences in the effective wave velocity, and in the travel time delays between effective velocities with and without a pump source.

Lay summary

The science behind how seismic waves propagate in rock to cause earthquakes, or how to predict damage in materials used in engineering, is still undergoing active research. The current view is that the inner structure of rock contributes to these phenomena. One way to study this is by sending sound waves through a sample of rock and measuring how the wave changes. We can easily imagine dropping a pebble in a still lake and seeing waves ripple outwards, and it is simple to imagine how those waves will change as they travel through the water. In comparison, a sound wave traveling through a rock will undergo much more complex behaviour. This complex behaviour depends on the composition of the rock as well as an aspect called nonlinearity.

Previous researchers have used different methods to study nonlinearity which involve using waves to analyze a sample. A wave called the pump wave is sent into the sample for either a short period of time, comparable to poking the sample, or a much longer period of time, comparable to pushing repeatedly on the sample. The complex behaviour we see changes based on which of these types of waves is used, and little research has been done to see if the two situations are comparable.

In this work, we use a programming code to model a rock with waves being broadcast into it, and change whether the pump wave is being broadcast for a long or short period of time in order to match the two methods used in experiments. A second wave, called the probe wave, is sent into the rock and interacts with the pump wave, allowing us to measure wanted parameters. We study the nonlinearity by looking at the speed at which the probe wave travels through the rock and the time this takes, and compare our results between the two methods of broadcasting the pump wave for short or long periods of time. We show that the method used does significantly change the measured nonlinearity and conclude that our model can be applied to both methods, but only when using a distinct model setup for each method.

Acknowledgements

I would like to extend my gratitude to Dr. Kris Poduska and Dr. Alison Malcolm for all of their support and guidance with my work, both during this honours project and during the summers beforehand. They have both been incredibly kind and open whenever I needed advice or help, and are great supervisors. Thanks to Jacob and Drs. Melnikov, Zheglova, and Tadavani for suggestions during group research meetings. I would also like to thank Dr. Rick Goulding, who has been there for me since I first stepped into his *Introductory Physics I* class during my first semester at Memorial University. Thank you to all of my professors from the Department of Physics and Physical Oceanography and the Department of Mathematics and Statistics for providing me the knowledge and inspiration that led to this honours project.

I thank Compute Canada and ACENET for allowing me to run my simulations on their remote servers and teaching me how to do so. Finally, I thank the Natural Sciences and Engineering Research Council of Canada for the Undergraduate Student Research Awards, which supported me in developing my research abilities, including the start of this current work.

Statement of contribution

The finite difference code used in my work has been developed and used by prior researchers. I have modified, refined, troubleshooted, and added new tools to the code including for visualization purposes. All of the data presented has been generated by me through this code. My co-supervisors Dr. Poduska and Dr. Malcolm have provided guidance to me throughout this honours work, including introducing me to the theory of elastic nonlinearity, and providing their opinions on many of my results. They have also given suggestions on the organization of this thesis. I have taken into account the advice of Dr. Poduska and Dr. Malcolm, but I have decided myself which aspects of my data are the most meaningful for this work, and developed my own explanations of my results.

Table of contents

List of tables

List of figures

List of symbols

$\boldsymbol{\epsilon}$	strain
$\boldsymbol{\sigma}$	stress
v_{pump}	velocity of the pump wave
v_{probe}	velocity of the probe wave
$v_{control}$	spatially averaged velocity with no pump
$v_{interaction}$	spatially averaged velocity with pump
$\boldsymbol{S}$	stiffness tensor
$\boldsymbol{C}$	compliance tensor
Δu	displacement discontinuity
t	traction vector
$\langle r \rangle$	spatial average of a variable r
x, y, z	positions along x-, y-, and z-axes of model respectively

List of abbreviations

DAET	Dynamic Acousto-Elastic Testing
FFT	Fast Fourier Transform

Chapter 1

Introduction

The field of nonlinear acousto-elastic behaviour in materials such as rocks is an area of active research with many important applications. The micro-structure of a rock, which may depend on fractures, cracks, density changes, or an external stress, can cause large scale phenomena such as earthquakes or the movement of fluids [1]. One of the intended goals of acousto-elastic testing is to characterize this micro-structure, which may aid in earthquake prediction and prevention of material fatigue in engineering.

The nonlinearity appears in the form of a nonlinear relation between the stress and strain fields within the rock. In a linear relation, the stress and strain are directly related by a tensor, as in Hooke's law. In the nonlinear case, the stress also depends on higher orders of the strain [1].

In nonlinear experiments, a strain field is set up within a sample, often by using an elastic pump wave. An elastic probe wave is then broadcast into the sample. The probe wave is perturbed by the strain fields due to the nonlinear nature of the sample, and the measurement of this perturbation, combined with information about background material parameters, may be used to determine some elements of the micro-structure.

Numerous theories exist to describe this nonlinear behaviour. I focus on two experimental configurations which involve both a probe wave and a pump wave; Dynamic Acousto-Elastic Testing (DAET) [4] uses a resonant pump wave, while modified non-resonant DAET uses a transient pump wave [1]. In this situation, transient means that the wave is only broadcast for a brief period of time. I numerically model a sample including a crack, and observe how changing certain parameters affects how the two waves interact within the sample. I aim to compare the two configurations and determine if they are compatible with each other and with my model.

1.1 Theory

1.1.1 Background

Nonlinear acoustics has seen active study for decades, for as long as researchers have been able to generate the needed acoustic waves. At its most basic, this nonlinearity arises from an extension of the linear Hooke's law, which relates the stress $\boldsymbol{\sigma}$ to the strain $\boldsymbol{\epsilon}$ as

$$\epsilon_{ij} = S_{ijkl}\sigma_{kl}, \tag{1.1}$$

where S_{ijkl} are the elements of the fourth-rank compliance tensor $\mathbf{S}$, σ_{kl} are the elements of $\boldsymbol{\sigma}$, and ϵ_{ij} are the elements of $\boldsymbol{\epsilon}$, noting that the stress and strain are both tensors. The nonlinearity involves expanding the stress in higher orders of the strain, which represent the interactions between probe and pump waves due to this nonlinear property of the material [1]. It has been found that materials such as rocks have an intrinsic nonlinearity, and that the presence of cracks or fracture networks in the sample significantly increases this nonlinearity [7].

Nonlinear acousto-elastic techniques in general have benefits over other methods of determining the micro-structure and nonlinear elastic behaviour of rock samples. A major benefit is that these techniques are non-destructive, requiring only external sources and receivers, without needing to fragment or crush a sample as may be needed when using a microscope to scan for fractures [2]. Relative variations in nonlinear parameters tend to be much higher than those in linear parameters when a sample is under stress, thus making them easier to detect.

There are numerous theories and experimental setups used to explore the nonlinearity of rocks. Quasi-static methods consist of applying a constant stress to a sample and broadcasting a high frequency probe wave through it to determine how the velocity, or speed of sound, varies throughout the medium as we change the applied stress. The stress is increased in discrete steps, and generally consists of pure tension or pure compression. Since the applied stress is quasi-static, values are averaged over an acoustic cycle in order to determine wanted parameters such as the elastic moduli of the material [2]. A more recent technique uses dynamic stress instead of a static applied stress. A low frequency pump wave is used to create a dynamic stress field in the sample, with which the probe wave interacts. This has the benefit of being able to measure parameters at all points in the acoustic cycle, giving more detailed results without the need for averaging. We explore two dynamic theories in detail. The first is Dynamic Acousto-Elastic Testing (DAET), using a resonant pump wave. The second is non-resonant DAET [1], where only a few cycles of a pump wave are used. The former is fairly well-studied, whereas the latter method has seen little research.

The use of nonlinear techniques has led to several observations of nonlinear behaviour. When a sample is stressed it often undergoes conditioning, with an elastic softening as soon as a small dynamic strain is applied, as a result of changes in the elastic moduli [4]. Another related behaviour is slow dynamics. When increasing stresses are applied to a sample, it may obtain a metastable state, requiring progressively longer periods of time to return to its original state [4]. Hysteresis is often observed in the change of stress as a function of the strain [8] when slow dynamics occur in a sample. The nonlinearity is also observed at very low strains, making almost all waves produce nonlinear effects in rocks.

1.1.2 Dynamic Acousto-Elastic Testing

Dynamic Acousto-Elastic Testing, or DAET, was developed and explored over the past two decades by Renaud [3] and Rivière [4], among others. The experimental setup is as follows, shown in Figure 1.1 [4]. A cylindrical sample with length larger than diameter is stood on a low frequency source that can compress and produce a strain field oriented along the length of the sample. A receiver is placed on the opposite face of the sample to measure this signal. A high frequency source and receiver are placed at a height just above the base of the sample, normal to the sample axis. The high frequency probe sends out pulses, establishing a baseline from the stress and strain within the sample. Next the low frequency pump is turned on and allowed to broadcast until a resonant state or steady-state is reached. The probe continues to send pulses, interacting with the established strain fields from the pump wave. These interactions are studied over a region that is much shorter than the pump wavelength.

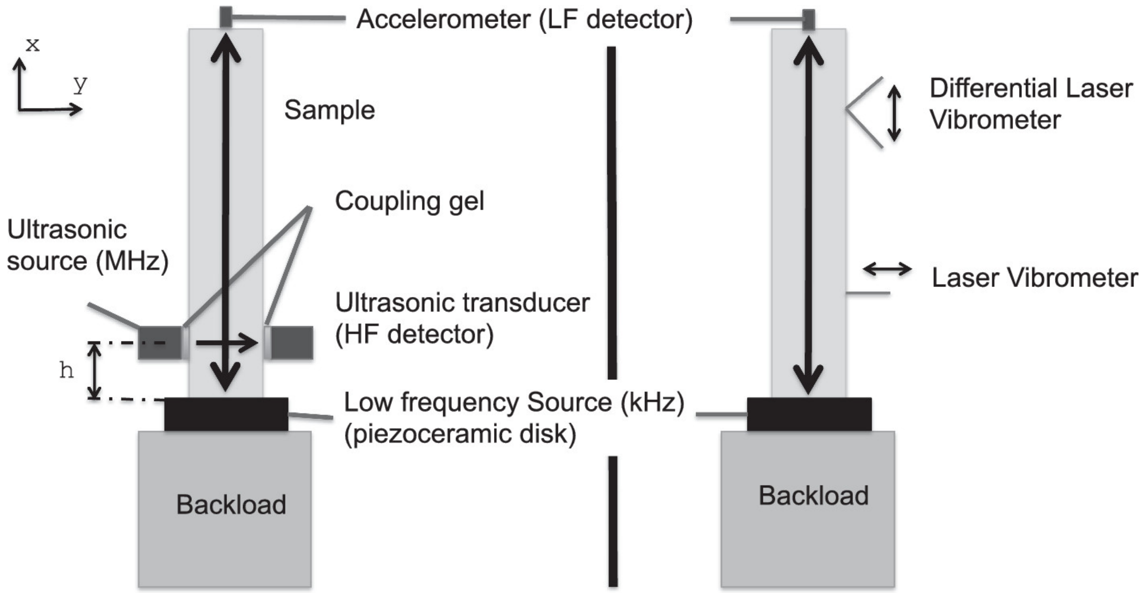

(a) DAE Setup (b) LF Field Characterization

Figure 1.1: A model setup for DAET experiments used by Renaud and Rivière. (a) shows the low frequency pump source upon which the sample rests. The high frequency probe source and receiver are supported on either side of the sample. Reprinted from [4], with the permission of AIP Publishing.

To allow the use of DAET, two requirements must be met. The pump strain field must be quasi-homogeneous in the region of interaction of the probe, and also quasi-static relative to the travel time of the probe.

Two of the commonly measured parameters in DAET are the time of flight modulation, which is the difference in travel time for the probe with and without the pump, and from which the relative velocity change can be calculated; as well as the low frequency acceleration, which measures the acceleration over time at a given point in a sample due to a low frequency source, and is related to the strain [4]. In some situations such as monitoring material damage, a more sensitive parameter is needed. This is the attenuation of the probe wave, reflected in the change in probe wave amplitude.

1.1.3 Non-Resonant DAET

Non-Resonant Dynamic Acousto-Elastic Testing was developed by Gallot [1] and also used by TenCate [9]. This method may be a better option for field research, as it does not require a standing wave to be produced within the sample; it instead relies on studying transient behaviour. There are two major differences from the standard resonant DAET and other similar theories. The setup still involves a high frequency probe wave whose propagation is disturbed by a low frequency pump wave. Instead of setting up a standing wave in the sample with the pump, only a few cycles are used, so transient behaviour is observed [9]. Unlike in DAET, the pump wave in non-resonant DAET is a transverse shear wave (S-wave), propagating orthogonally to the probe wave, which is a compressional, longitudinal wave (P-wave). Due to these differences and the lack of research using this method, it is uncertain if results found using this method are comparable to results found using DAET.

The experimental setup is as follows [1]. A sample is placed upright on one of its rectangular faces. An S-wave source is placed on the top face of the sample, broadcasting down into the sample. A P-wave source and a receiver are placed on opposite faces of the sample, with axes normal to that of the S-wave source. As before, the S-wave pump has a low frequency and high amplitude, while the P-wave probe has a high frequency and low amplitude. A transmission delay between the broadcast of the P-wave and the broadcast of the S-wave is then used. Changing the transmission delay changes the phase of the pump wave when the probe wave interacts with it, which may cause changes in the velocity or time delay. I do not explore a change in transmission delay in the current work.

The main parameter of interest is the propagation time delay of the probe as a function of the transmission delay. This delay is found by a cross-correlation between a measured pulse generated without a pump wave and a perturbed pulse generated with a pump wave. The effect of fracture networks is also investigated by performing the experiment with different orientations of the sample [9]. One useful observation is that waves passing through a crack cause that crack to open and close in a continuous manner, while the waves themselves are also perturbed by the crack [5].

1.1.4 Linear Slip Theory and Effective Medium Theory

In order to quantify the effects of the crack on my model, I use linear slip theory, developed largely by Schoenberg [6] and chosen due to the relative ease in modeling it. The theory applies to the case of an interface between two materials that are imperfectly bonded, such as a crack or fracture inside of a rock. The displacement of a wave across this interface is discontinuous. This theory posits that the discontinuity Δu is linearly dependent on the traction stress t, taken to be continuous across the interface. That is, $t = \mathbf{C}\Delta u$, where $\mathbf{C}$ is a stiffness tensor. For simplicity, the compliance tensor $\mathbf{S} = \mathbf{C}^{-1}$ is often used, giving $\Delta u = \mathbf{S}t$ [6]. Since our crack is symmetric, the compliance tensor only depends on two values, the tangential and normal compliances.

When used in conjunction with effective medium theory [7], linear slip theory allows for the calculation of the average strain in a sample as depending on the compliance tensor of the background material, the average stress, and an integral over the displacement discontinuities of all cracks. The background material is the part of the sample where there is no crack. The total effective compliance of the material can also be calculated simply as the sum of the background compliance and the compliances of the cracks. In comparison, using the stiffness would require summing over reciprocals, justifying the use of compliance over stiffness tensors.

Using effective mean theory allows for a generalized linear Hooke's law [5] to be used as

$$\langle \epsilon_{ij} \rangle = \langle S_{ijkl} \rangle \langle \sigma_{kl} \rangle, \tag{1.2}$$

where $\langle\rangle$ represents a spatial average. This follows the form of the usually linear Hooke's law as in equation 1.1, except now we use the effective stress, strain, and compliance tensors as the averages of the stress, strain, and compliance. The volume over which they are averaged is the yellow cube shown in Figure 2.1 at the start of the next chapter, covering $x = 0.05$ m to $x = 0.1$ m, $y = -0.025$ m to $y = 0.025$ m, and $z = 0.05$ m to $z = 0.1$ m. This is the region where the probe wave, pump wave, and crack should interact most strongly, and is chosen so that the averaged stress and strain are not zero [5]. The crack itself is centered at $x = 0.05$ m, $y = 0$ m, $z = 0.07$ m with radius 0.005 m and normal along the z-axis.

Chapter 2

Computational Methods

2.1 Model Initialization

I present my numerical model of nonlinear wave propagation, first making some comments on its development. This model has been previously used by Rusmanugroho et al [5], and is written in a mix of Matlab and C code. An NSERC Undergraduate Student Research Award that I was granted allowed me, over the course of 16 weeks, to explore, expand, and refine the model. The work done includes locating and minimizing sources of error in the code, ensuring it runs smoothly and efficiently in a repeatable way, adding new ways of visualizing and storing the output data, and reducing the likelihood of subtle user-induced error leading to discrepancies in the data. More fundamentally, I explored how the model works and what it represents physically, leading to a better understanding of both the theoretical and experimental aspects of this field of research. For the purpose of this thesis, I use this model to answer research questions about how the presence of cracks in a medium affects the resonance and non-resonance behaviours.

I begin by creating a 3-dimensional lattice with equal spacing in each direction to form our medium, shown in Figure 2.1. The default model has lengths of 0.15 m,0.05 m, and 0.15 m along the x-, y-, and z-directions respectively. I prescribe 6 independent parameters to the medium to specify its properties, with their values listed in Table 2.1. These include its density of 2285 kg/m^3, the P- and S- wave speeds, and the 3 nonlinear Landau-Lifshitz parameters as defined in [5]. All 9 components of the linear

Parameter	Value
P-wave speed	2954 m/s
S-wave speed	1829 m/s
Density	2285 kg/m^3
A (Landau-Lifshitz)	-8.725×10^{11} N/m^2
B (Landau-Lifshitz)	$-1.176\,25 \times 10^{12}$ N/m^2
C (Landau-Lifshitz)	-6.7375×10^{11} N/m^2

Table 2.1: Initial parameters used to specify properties of the medium. These values have also been used by Rusmanugroho [5].

stiffness tensor are calculated from the P- and S-wave speeds. This uniquely specifies the properties of a nonlinear, homogeneous medium.

A circular crack with radius 5 mm is added with center at position (0.075,0,0.070) m with normal along the z-direction. The density and P- and S-wave velocities of the medium are used along with specified crack parameters to create a distinct stiffness tensor for the crack itself.

Depending on which simulation is being done, sources are next added to the model to produce the waves. All sources are circular with a radius of 1 cm. All simulations have a P-wave probe source, by default centered at position (0.075,0,0) m with normal in the z-direction. A sinusoidal wavelet is defined with a frequency of 5×10^5 Hz and amplitude of 1×10^{-4} N/m^3 with a single cycle. If needed, an S-wave pump source is added, by default centered at position (0,0,0.075) m with normal in the x-direction. A sinusoidal wavelet is defined with a frequency of 5×10^4 Hz and amplitude of 1×10^{-2} N/m^3, and we use a range of 1 to 100 cycles. Examples of these source waves are shown in Figure 2.2.

To record data during the simulation, I use 6 recording slices, all of which are squares lying parallel to one of the sides of the medium. These 6 slices form a cube centered at (0.075,0,0.075) m with a side length of 0.05 m, shown in Figure 2.1. When averaging of the strain and stress is performed using effective medium theory, this is the representative volume over which the averaging occurs. Parameters such as stress and strain are recorded throughout the simulation on these slices. The data are also recorded along a segment of the crack itself, from the center of the crack out to a radius of 1 mm.

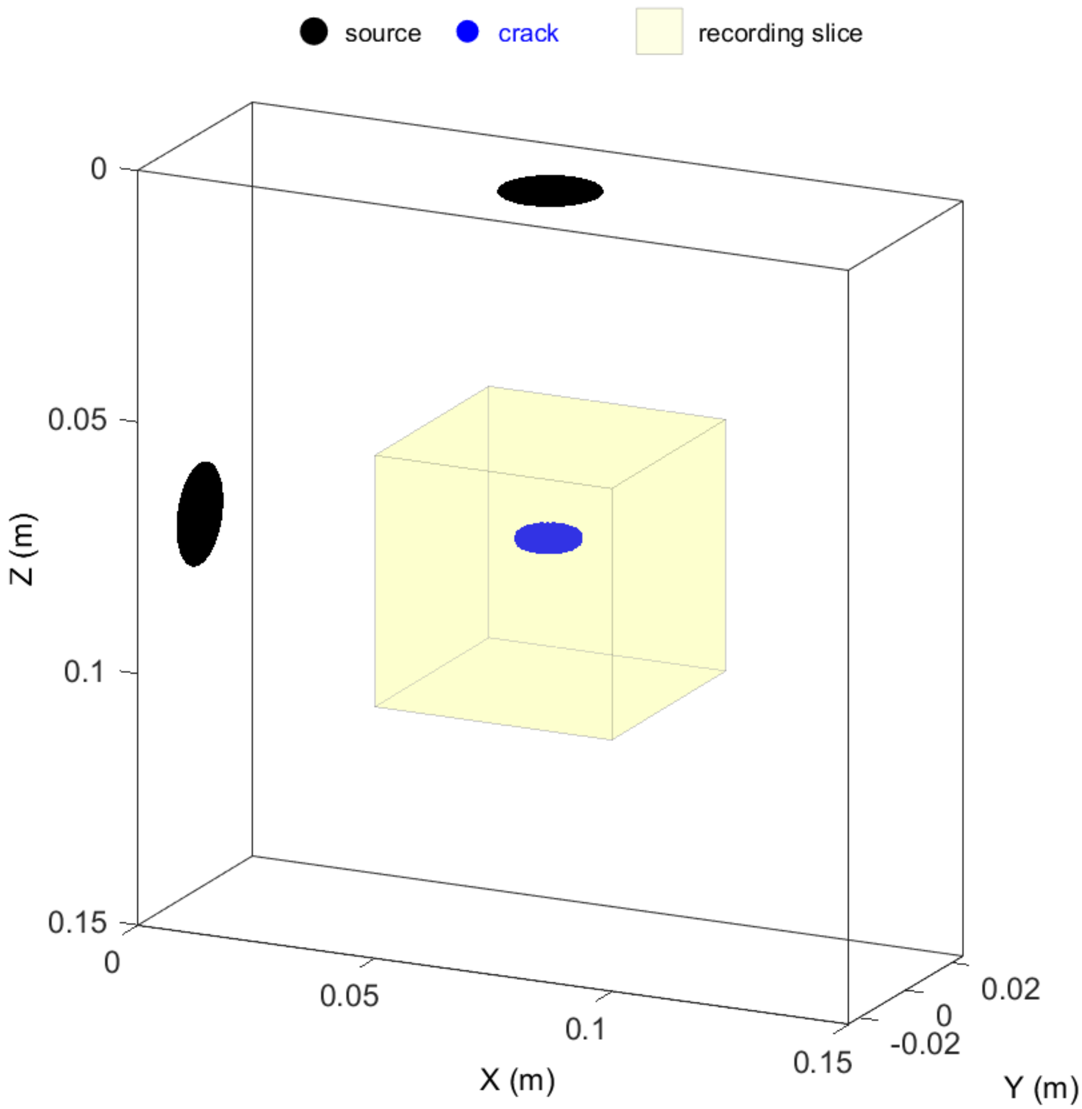

Figure 2.1: The default model used with two sources, shown in black. The probe source is on the top face along $z = 0$ m, and the pump source is on the face along $x = 0$ m. The crack is shown in blue along $z = 0.07$ m. The yellow cube is the volume over which averaging of the strain and stress is performed, with each face called a recording slice.

A total simulation time is set, at 1.0×10^{-3} s for most simulations. It is split into time steps of 2.5×10^{-8} s. The parameters of interested are recorded after every 100 time steps for most simulations to speed up the process, without losing any important fine detail.

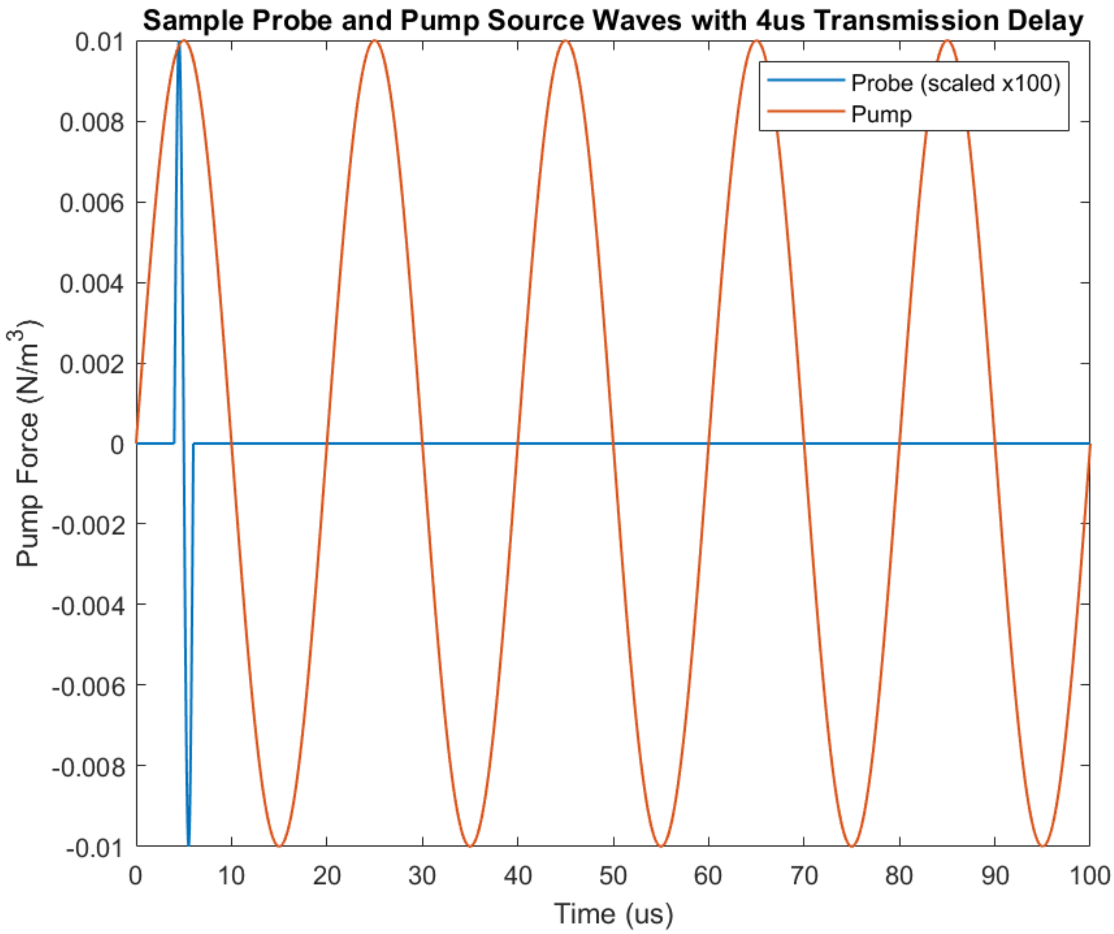

Figure 2.2: A sample of the source waves for the probe and the pump when a transmission delay of $4\mu s$ is used. Note that the amplitude of the probe wave has been multiplied by a factor of 100 so that both waves are visible. This presents 5 cycles of the pump wave, and the single cycle of the probe wave.

2.2 Computational Details

A 4th order time domain finite difference in Cartesian coordinates is used to model the wave propagation. This is an iterative method in which the modelled parameters are updated at alternating time steps, and the Cartesian coordinate system is used. A displacement vector in a region around each point is used to estimate the directional derivatives of the displacement at that point, which is then used to calculate the updated strain. A similar calculation is used to find the directional derivatives of the velocity, which along with the displacement derivatives allow the first Piola-Kirchhoff stress to be updated. On alternating time steps, the stress derivatives are used to calculate the velocity and displacement. A free boundary condition at each surface is maintained at each step. This finite difference portion of the code was written around a decade ago and has been used and modified since by numerous researchers. Many of the equations being modelled here have been presented by Rusmanugroho [5], who previously worked with this finite difference code.

A note must be made on where the code itself is run. For efficiency, it has been designed to run on remote nodes using parallel computation. These remote nodes are run by ACENET in partnership with Compute Canada, who allowed me to run my code on the Torngat server via the Siku regional system. I can connect to these remote servers directly from my own computer. Access to this server is what made my computations feasible. Instead of simulating and updating the entire model on my computer, which would likely take days, the model itself is divided into slices of constant z-coordinate. Parallel computation allows each section of the model to be simulated on a given remote node, with all nodes working simultaneously. There is some overlap for communication between the nodes. This reliably brings computational time down to a few hours, and using more nodes will increase the speed. However, a subtle issue arises from the positions of the sources. Recall that the pump source has normal along the x-direction. Depending on exactly how the model is sliced for parallel computation, this source may be split over multiple nodes. Despite the node overlap, changing how the source is split over nodes does affect the resulting calculated control effective velocity rather noticeably. After finding this source of error, I modified the setup slightly to ensure that the source is always split the same way for every simulation to be certain my results are all comparable to each other.

2.3 Effective Velocity Calculation

The data from the recording slices and receiver are used to calculate an effective velocity. When only the probe is used I call this the control effective velocity, denoted $v_{control}$, and when both probe and pump are used I call this the interaction effective velocity, denoted $v_{interaction}$. Refer to Table 2.2 for a brief summary of the types of velocities that occur in my work. All components of the stress in the z-direction are multiplied by either a normal or tangential compliance. The background stiffness tensor and nonlinear parameters are needed. The discontinuities in the displacement

Notation	Velocity Type	Meaning
v_{probe}	Probe velocity	For sinusoidal wave broadcast from probe source, high frequency.
v_{pump}	Pump velocity	For sinusoidal wave broadcast from pump source, low frequency.
$v_{control}$	Control effective velocity	Spatially averaged from setup with only probe.
$v_{interaction}$	Interacting effective velocity	Spatially averaged from induced-strain setup with probe and pump.

Table 2.2: Definitions of the four types of velocity examined in this work.

across the crack are integrated and summed to give the product of the average compliance of the crack with spatially averaged stress [5]. The recording slices are used to calculate the average or effective stress and strain, which allow for an effective stiffness tensor to be found. Inverting this gives an effective compliance tensor, to which the average compliances are added. Inverting once again gives the final effective stiffness tensor. Dividing the appropriate component by the medium's density [5] gives the effective velocity.

2.4 Time Delay Calculation

With the effective velocities calculated, the next step is to calculate the travel time delay between the two simulations, with and without a pump source. This is done by simply adding the travel time through each lattice step along the x-direction as the grid size divided by the velocity at that point. The travel time for the probe-only simulation, with the control effective velocity, is subtracted from that of the probe and pump simulation, with the interaction effective velocity. This gives the time delay, which is induced by the strain fields set up by the pump wave.

Chapter 3

Results

3.1 Control Effective Velocity

For every simulation, I first used a setup with only the probe and no pump. This allows for the calculation of a time delay when compared to a simulation with both sources. The only parameter that changed is the initial transmission delay, which simply determines at what time in the simulation the probe starts broadcasting. Changing this delay does not affect the behaviour of the control effective velocity $v_{control}$, serving as a verification that the code is working as intended.

I start with a brief explanation of what I mean here by control effective velocity, $v_{control}$. The probe source broadcasts a single cycle force wave into the medium, consisting of alternating compressions and rarefactions of particles within the medium. As this initial sinusoidal wave propagates, the intrinsic nonlinearity of the medium distorts the wave, and this effect is amplified as it interacts with the crack. The propagating wave produces strain and stress fields in the medium. Reflections off the far boundary may also add to this distortion. As described above, using linear slip theory and effective medium theory, the stress and strain fields are averaged in a way as to include the perturbations due to the crack, producing an effective homogeneous medium. From this, the probe velocity v_{probe} as it would occur in the effective homogeneous medium is calculated and called the control effective velocity. This is an example of a phase velocity, a measure of how fast any wave will travel though the medium, and a property of the medium. The effective velocity is constant

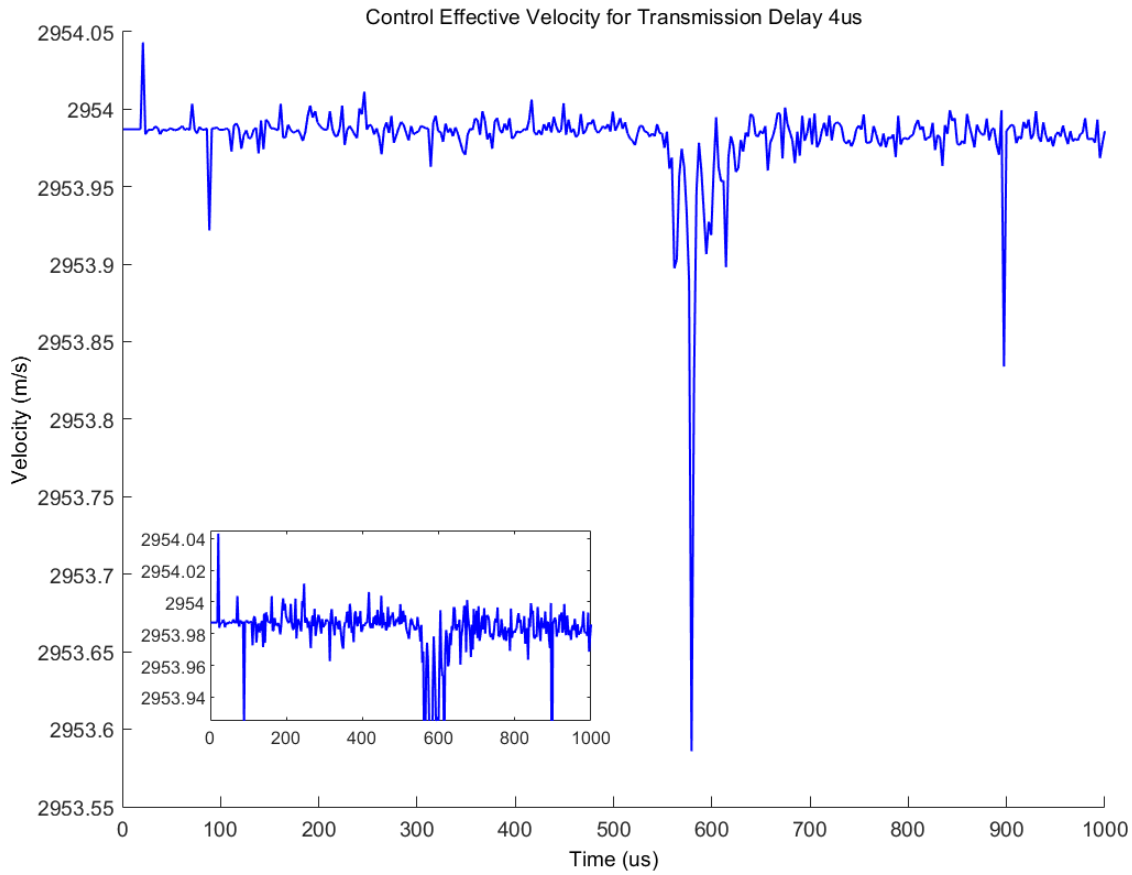

Figure 3.1: The control effective velocity from a simulation with a probe source and no pump, including a transmission delay of 4μs. The inset plot expands on a small velocity range around the mean, showing the finer details.

throughout the representative volume. In comparison, the interaction effective velocity $v_{interaction}$ is calculated through the same procedure, except I add the pump source to the medium, which sets up strain fields throughout the sample which perturb the probe wave. $v_{interaction}$ is the probe velocity as it would occur in the effective homogeneous medium derived from this new setup. Both effective velocities measure the same parameter, and I use 'control' or 'interaction' to distinguish between the setups used before averaging.

Next, I describe the velocity as it changes in time. With the addition of the pump wave, the stress and strain fields throughout the medium will be perturbed, and will change as the pump and probe waves interact with each other and with the crack. This will then cause the calculated effective velocity to vary from the control case with no pump source. Thus, we will also see a delay in the travel time of the wave, which is another aspect of the nonlinearity I study in this work.

Figure 3.1 shows $v_{control}$ when the simulation includes a probe and no pump. A transmission delay of 4μs was used, resulting only in a shift along the horizontal axis. Note that since the pump is not used, this velocity is the same for every simulation with the same model geometry as the properties of the probe are fixed across all of these simulations. The velocity is initially small for a short period after the probe starts, quickly devolving into what appears to be noise with an amplitude range of around 0.05 m/s on average, very small compared to what we later see for the interaction effective simulation. There does not appear to be any underlying frequency or oscillation. Two notable peaks occur in the form of a drop in velocity, of much larger amplitude than for the rest of the simulation time. The first has an amplitude of around 0.4 m/s while the second has a sharp decrease with an amplitude of 0.25 m/s, an order of magnitude larger than average. The time at which the peak occurs suggests that it might be a result of reflections off the far boundary of the medium interacting with the incoming waves at the crack. This represents linear behaviour of the material for the probe.

3.2 Varying Number of Pump Cycles

The first major parameter I varied was the number of cycles for which the pump broadcasts. Previous simulations used 3 cycles. I performed simulations for 1, 2, 3, 18, 20, 22, 24, 26, 50, and 100 cycles, observing how the velocity changes, and deciding which choice best simulates a resonant condition.

For 1, 2, and 3 cycles, with $v_{interaction}$ for 3 cycles shown in Figure 3.2, we see no clear frequencies in the interaction effective velocities, resembling little more than noise. Increasing the number of cycles gives behaviour similar to beats, with maximum amplitude changing smoothly at a low frequency along with high frequency oscillations of the velocity. The data for 18, 20, 22, 24, and 26 cycles are similar in amplitude and frequencies, with that for 20 cycles shown in Figure 3.2. The maximum amplitude relative to the mean is around 0.25 m/s, and the mean is constant for all simulations and effectively constant throughout each simulation. Each of the five simulations have an identical velocity for the first 350μs. After this point, each simulation begins to diverge slightly from the simulations with more pump cycles. This is a trend that

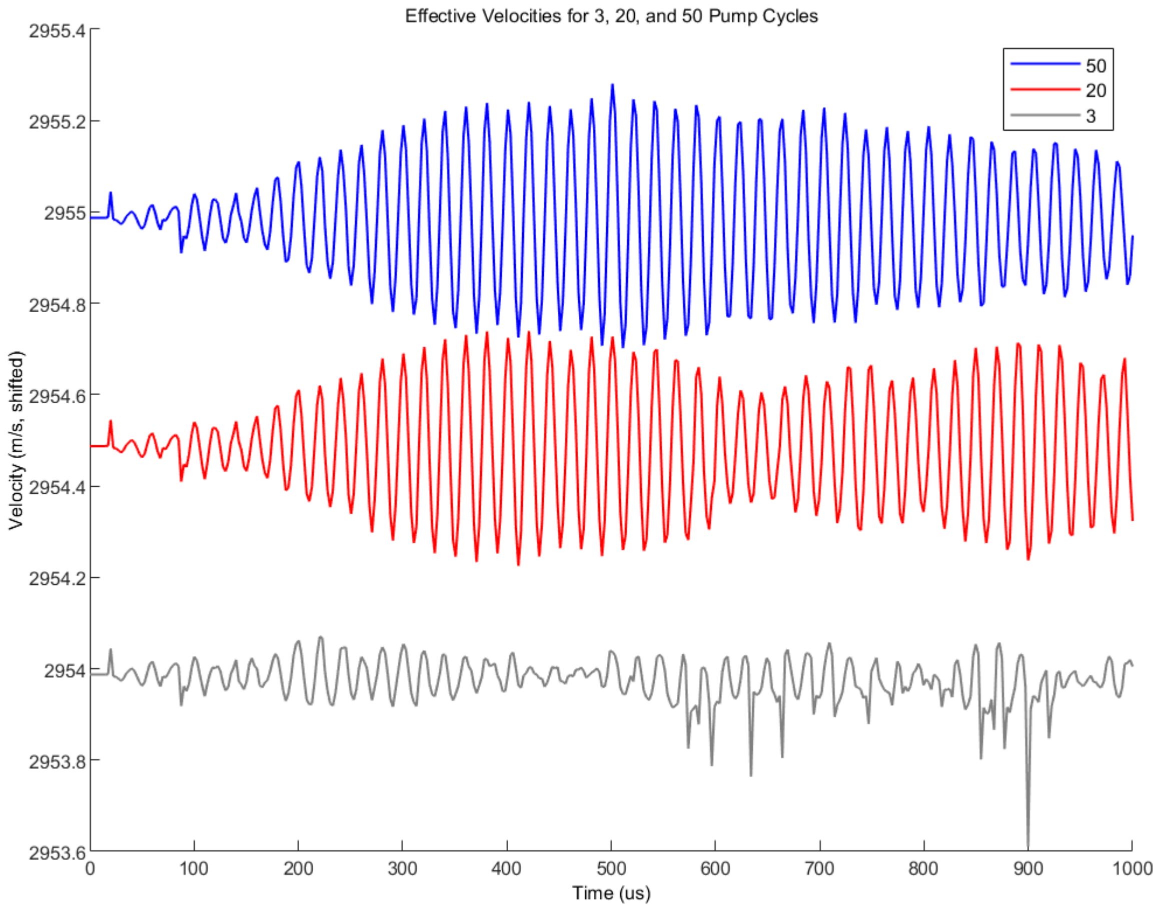

Figure 3.2: Interaction effective velocity, showing results for 3, 20, and 50 cycles of the pump. The 20 cycle data have been shifted upwards by 0.5 m/s and the 50 cycle data have been shifted upwards by 1.0 m/s for clarity. Note the appearance of a smooth change in maximum amplitude.

continues up to 50 cycles, with the effective velocity data matching for more of the simulation time as the cycles increase. I show results for 3, 20, and 50 cycles in detail in Figure 3.2 as mentioned. I note that the range for $v_{interaction}$ is on the order of 0.5 m/s, compared to the average range for the control effective velocity, which is on the order of 0.05 m/s or an order of magnitude smaller. For fewer than 50 pump cycles, the pump stops broadcasting before the end of the simulation, leading to potential changes in effective velocity as the stress decreases. This effect is not seen for these simulations, with no appreciable deviation from the oscillations.

Using 50 pump cycles corresponds to broadcasting the pump for the entire simulation, 1000μs. We observe the trend from before again, which can be seen as $v_{interaction}$

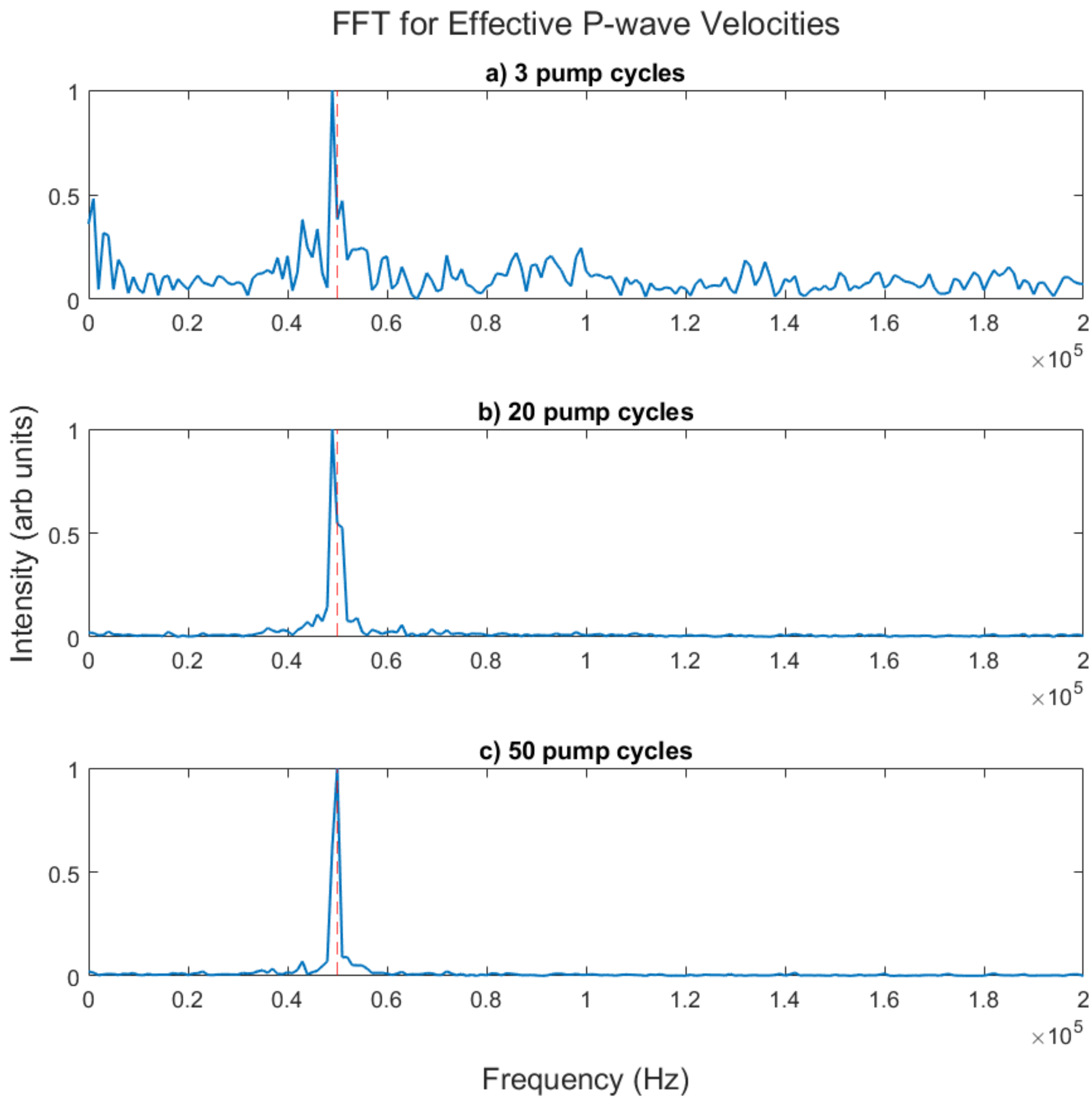

Figure 3.3: The Fast Fourier Transforms (FFT) for interaction effective velocities using 3, 20, and 50 pump cycles in (a), (b), and (c) respectively. The vertical axis is the normalized intensity in arbitrary units. The dashed red line at 5×10^4 Hz is the pump source frequency.

converging to that of a permanently broadcasting pump as the number of cycles increases. While the maximum amplitude of the wave does not change from previous simulations, it changes more gradually in time, more closely resembling the desired resonant state. We have a minimum velocity of 2954.7 m/s, and a maximum of 2955.3

m/s. I next perform a Fast Fourier Transform (FFT) on the data, recovering the underlying frequencies, which I show in Figure 3.3. For 50 cycles, in Figure 3.3.c, we find a single large frequency peak at 5×10^4 Hz, which is the frequency of the pump wave. This result is expected, as the pump wave has an amplitude two orders of magnitude larger than that of the probe wave, and I find from the FFT of $v_{control}$ that there are no frequency peaks; in particular, the probe frequency does not contribute to the effective velocity. Having a single well-defined frequency does not imply that this case must be a resonant or steady state, but it does suggest that the main indicator of whether a state is resonant is whether or not the maximum amplitude of the effective velocity varies in time.

Looking now at 20 cycles of the pump source, which means the pump is broadcasting for 40% as long as for 50 cycles, we see fairly similar behaviour to the 50 cycle case. As seen in Figure 3.2 and mentioned already, increasing the number of pump cycles causes $v_{interaction}$ to converge towards that of the 50 cycles case. We see oscillations at a high frequency, as well as what appears to be beats, with a smoothly changing maximum amplitude. Checking the FFT in Figure 3.3.b confirms that the main frequency is that of the pump wave, with no other frequency having a significant effect. The amplitude is less constant than in the 50 cycle case, implying that once the pump stops broadcasting, the reflections of the pump wave are not sufficient to preserve the maximum amplitude, which is expected. However, the amplitude does not decrease constantly, nor does it approach the behaviour $v_{control}$. Then the pump broadcasting for 20 cycles is sufficient to significantly perturb the amplitude of the effective velocity for the entire simulation.

I now compare the transient case of 3 pump cycles, similar to non-resonant DAET [9]. Looking at $v_{interaction}$ in Figure 3.2, it differs significantly from the cases with 20 and 50 cycles. For the first 400μs, there is a slight oscillation, which then loses its smooth shape, with numerous short drops in velocity and no clear frequency. The amplitude of the velocity remains small, with no clear growth or decay as the simulation progresses. Unlike the previous case, there is no smooth change in maximum amplitude, and the instantaneous amplitude sees sudden disjoint changes over very brief periods. The FFT in Figure 3.3.a shows that the main frequency is still the frequency of the pump wave. However, the relative intensity of this peak has decreased significantly, with a wide, non-negligible range of frequencies appearing in the data. The pump wave still affects the effective velocity, but no longer overwhelms the probe wave completely.

Finally, I perform a simulation with 100 cycles of the pump wave, which also requires doubling the simulation time to 2000μs. I find that $v_{interaction}$ is identical to that of 50 cycles for the time range for the first 1000μs of the simulation as expected from the prior trend, and that the maximum amplitude itself begins to oscillate, with the FFT showing peaks at 5×10^2 Hz, 5×10^4 Hz, 1×10^5 Hz, and 2×10^5 Hz. The velocity appears much less smooth than for 50 cycles, with spikes where $v_{interaction}$ decreases rapidly. It is not clear to me what causes the additional frequencies, and determining this could be something to explore in future work. Thus I decide to focus on simulations of 50 cycles as optimal for a steady state. It is less simple to determine if 50 cycles of the pump causes a resonant state, as that would also depend on matching the frequency of the source waves to a characteristic frequency of the medium. For the purpose of this work, I believe that the steady state is a sufficient approximation to true resonance. From this point forward, I study the steady state according to this understanding.

3.3 Varying Model Geometry

Having chosen 50 cycles of the pump wave, I compare three different model geometries and their effect on $v_{interaction}$. Geometry 1 is the one shown in Figure 2.1 and previously examined, with dimensions of 0.15 m, 0.05 m, and 0.15) m along the $x-$, $y-$, and $z-$axis respectively. Geometry 2 consists of doubling the length of the side along the x-axis, with dimensions of 0.30 m, 0.05 m, and 0.15 m. Geometry 3 similarly consists of doubling the length of the side along the z-axis, with dimensions of 0.15 m, 0.05 m, and 0.30m. Note that this means that the distance required for one of the sources to travel the length of the medium is also doubled; this is the probe for geometry 3 and the pump for geometry 2. The position of the crack does not change between any of the geometries.

In comparison, the cylindrical sample used in the resonant DAET experiment by Rivière [4] is approximated by a prism of with dimensions of 15 cm, 2.54 cm, and 2.54 cm, and so I expect that geometry 2 should best compare to this sample. This gives a ratio $x/y \approx 6$ in both cases, where my other two geometries have ratio $x/y = 3$. For comparison, the sample used by Gallot for non-resonant DAET [1] has dimensions

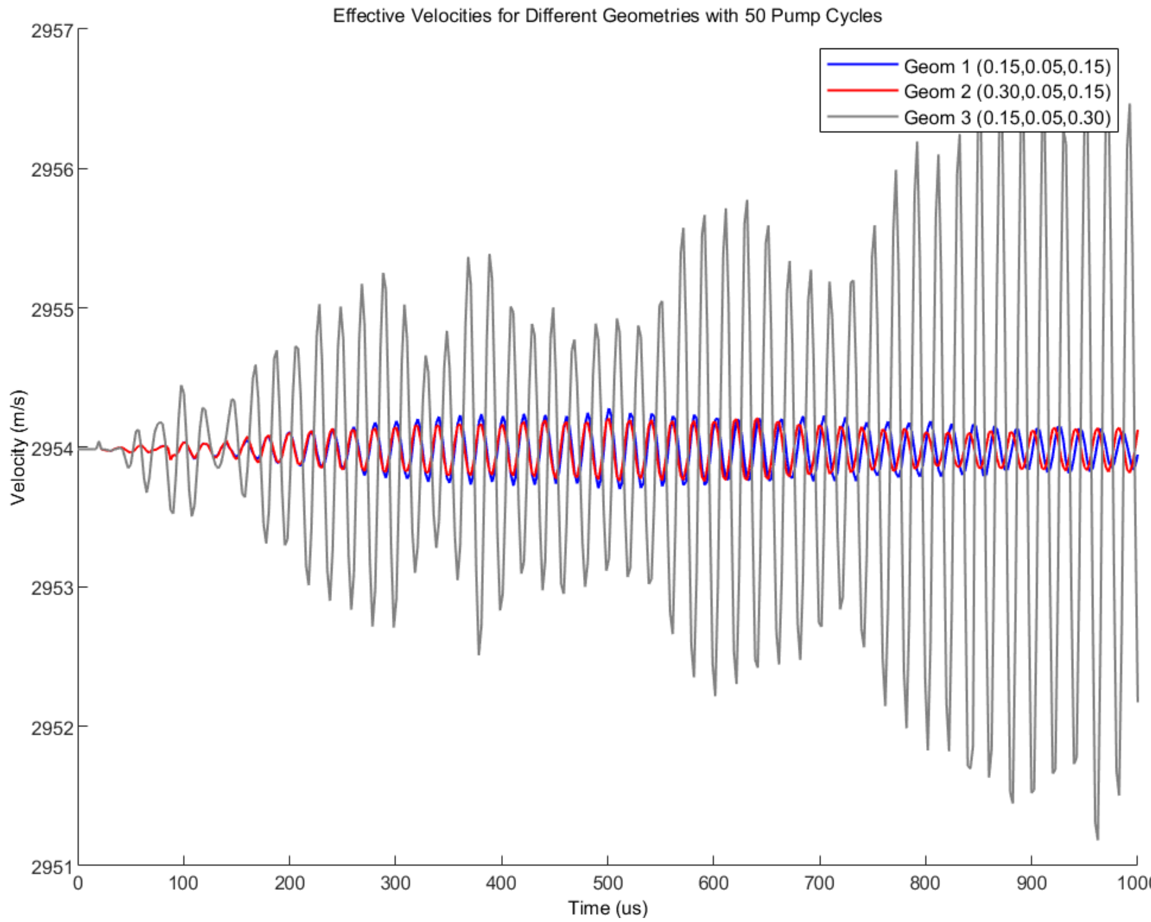

Figure 3.4: The interaction effective velocity when probe and pump are broadcast. Comparing results for 3 model sizes, with 50 cycles. Each tuple (x, y, z) in the legend refers to the dimensions of the model along the respective axes. Doubling the length along z leads to a non-smooth, increasing amplitude.

of 15 cm, 3 cm, and 15 cm for a ratio $x/y = 5$. The results from the three model geometries are seen in Figure 3.4.

We see that $v_{interaction}$ does not change significantly between geometry 1 and geometry 2. Note that this size variation corresponds to the direction in which the pump wave propagates. The amplitude decreases slightly from geometry 1 to geometry 2, and the two waves are slightly out of phase with each other, with peaks for the geometry 2 velocity occurring slightly earlier in time, while maintaining the same shape as the geometry 1 velocity. The phase shift may be caused by a slight shift in conditions needed for steady state when the model length is increased. This suggests that I can continue using my default, geometry 1, without needing to spare much consideration for the difference from the DAET sample sizes. This is useful, as the geometry 1 model takes less computational time to run, with only half as many lattice points as the larger two models.

Unlike the first variation, the model with geometry 3 sees a drastic change in $v_{interaction}$. With 50 pump wave cycles, the smooth amplitude changes in the velocity are lost, with more abrupt increases and decreases in amplitude. The overall oscillation amplitude appears to increase in time, with the amplitude being at least three times that of the amplitude for geometry 1, increasing to eight times at some points. We see that this new wave is also out of phase with the geometry 1 wave, with its peaks occurring at the same times as troughs for the latter wave. This size variation corresponds to doubling the direction in which the probe wave propagates. The large difference in velocity may be due to the pump wave no longer having a boundary from which to reflect at $z = 0.15$ m while still having a short distance to the opposite face at $x = 0.15$ m. This particular change may affect the pump wave reverberations in such a way as to cause the velocity to increase more similarly to a driven oscillator than a steady state.

3.4 Travel Time Delay

Once I get $v_{interaction}$ from the probe and pump, and $v_{control}$ from the probe alone, I can calculate the time delay between the two at each point along the z-axis of the medium by subtracting the travel time of the control wave from the travel time of the interaction wave. The results do not seem to match similar ones from Rusmanugroho [5], although I plot the time delay throughout a simulation for a single transmission delay, instead of plotting the maximum time delay over increasing transmission delays. This time delay is shown for 3, 20, and 50 cycles of the pump wave in Figure 3.5.

I start with 50 cycles, shown in Figure 3.5.c. Initially, the delay is zero, which is expected due to the 4μs transmission delay. The time delay then takes on a sinusoidal form with a distinct wavelength, about half the wavelength of the probe wave, but with increasing amplitude and increasing mean. That is, the two waves are fairly close in time to each other, but $v_{control}$ is beginning to increase relative to $v_{interaction}$. Then, around the middle of the model near the crack, the delay drops from a maximum of 0.027 ns and oscillates near -0.05 ns while keeping the same period, and the

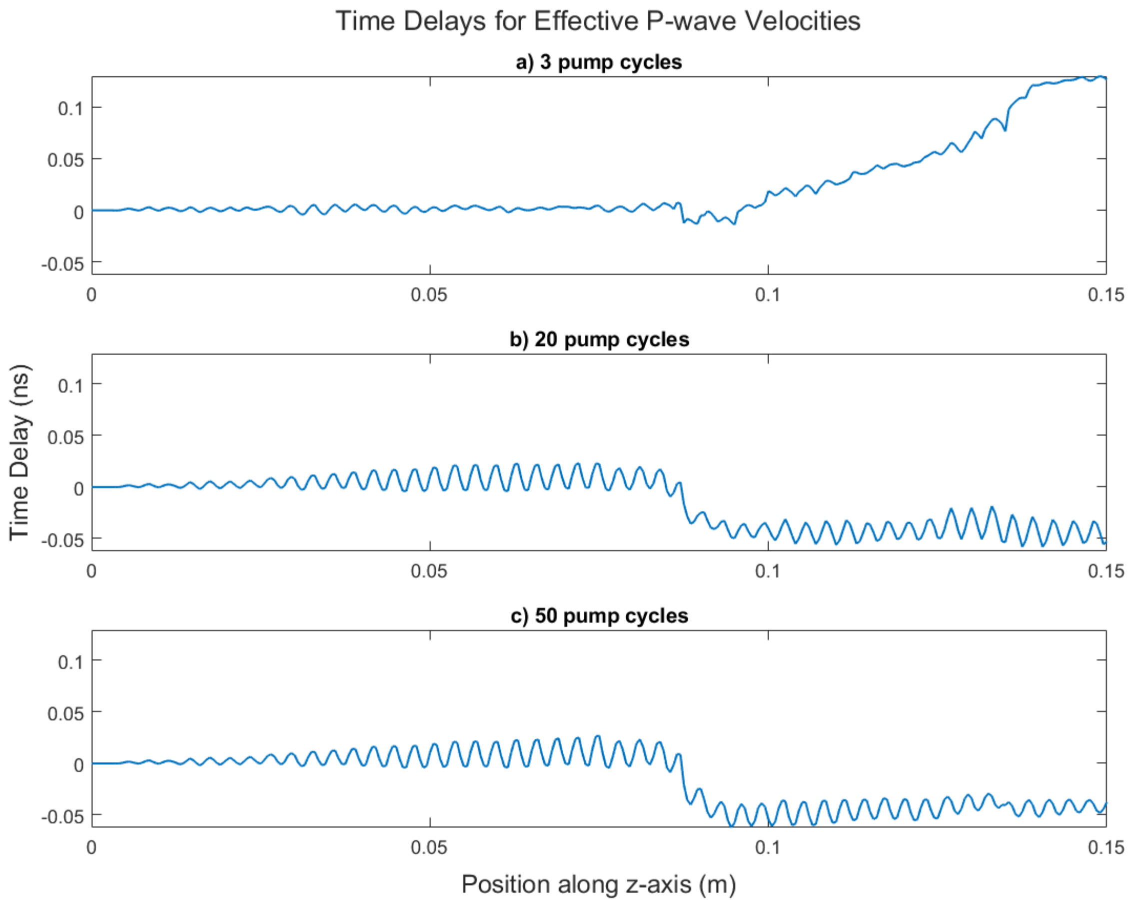

Figure 3.5: Plotting the time delays for interaction effective velocities using 3, 20, and 50 pump cycles in (a), (b), and (c) respectively. Note that the time delay is measured in nanoseconds.

interaction wave is now ahead of the control wave. After travelling slightly further along the z-axis, there is a sharp drop in time delay, which still oscillates around a negative time delay of -0.205 ns. This indicates that both waves are travelling at the same velocity, but that something caused a large temporary increase in $v_{interaction}$.

Comparing Figure 3.5.c with Figure 2.1, we see that the position along the z-axis at which the delay drops and becomes negative occurs very close to the position on the circumference of the pump source which is furthest from the probe source. Since the travel time for the probe does not involve the pump source at all, this implies that there is sudden, temporary increase in $v_{interaction}$, causing the travel time to decrease relative to the control effective wave. This shift is likely due to a change in the strain field between the region from $z = 0.06$ m to $z = 0.09$ m in which the influence of the pump is greatest, and the region just beyond the edge of the pump. The probe wave would be perturbed as it travels through the rapidly changing strain field, thus leading to a change in $v_{interaction}$ as well. It is somewhat surprising that the change isn't more gradual with the strain decaying away from the pump, and fully understanding this would require further investigation.

Largely similar behaviour also occurs in the time delay for 20 cycles, shown in Figure 3.5.b, as for 50 cycles. $v_{control}$ and $v_{interaction}$ are fairly similar, with the latter being very slightly faster. We again see a sharp drop where $v_{interaction}$ increases as the wave passes outside of the region through which the pump wave propagates. Beyond this point in the medium, the two wave velocities are roughly equal again. Throughout, $v_{interaction}$ is very slightly higher than $v_{control}$, leading to a minor decreasing trend in the time delay, which is the opposite trend as in the 50 cycle case. Since v_{probe} is identical in both cases, this means that increasing the time for which the pump is broadcast actually causes $v_{interaction}$ to decrease.

The time delay for 3 cycles, shown in Figure 3.5.a, is initially similar to that in Figure 3.5.c for 50 cycles. The delay oscillates, though not smoothly, and gradually becomes greater, with $v_{control}$ being very slightly greater than $v_{interaction}$. The delay drops and becomes negative as the interaction effective wave passes throughout the region of the pump and briefly increases in velocity. Beyond this point, the behaviour changes significantly from that of 50 cycles. The delay almost immediate starts to rapidly increase, doing so throughout the rest of the medium. The oscillatory behaviour also disappears. $v_{interaction}$ decreases sharply when not travelling through the region of influence of the pump, becoming much slower than the control effective wave.

3.5 Hysteretic Behaviour

3.5.1 Observations for 50 Cycles

One of the commonly observed properties of a nonlinear resonant experiment is hysteretic behavior, seen when plotting relative velocity change [4] or time of flight modulation [3] as functions of strain. Hysteresis generally occurs due to the effects of slow dynamics [8]. We see what appears to be a similar behaviour in my results, where I plot $v_{interaction}$ as a function of the effective strain, shown in Figure 3.6. I discuss this

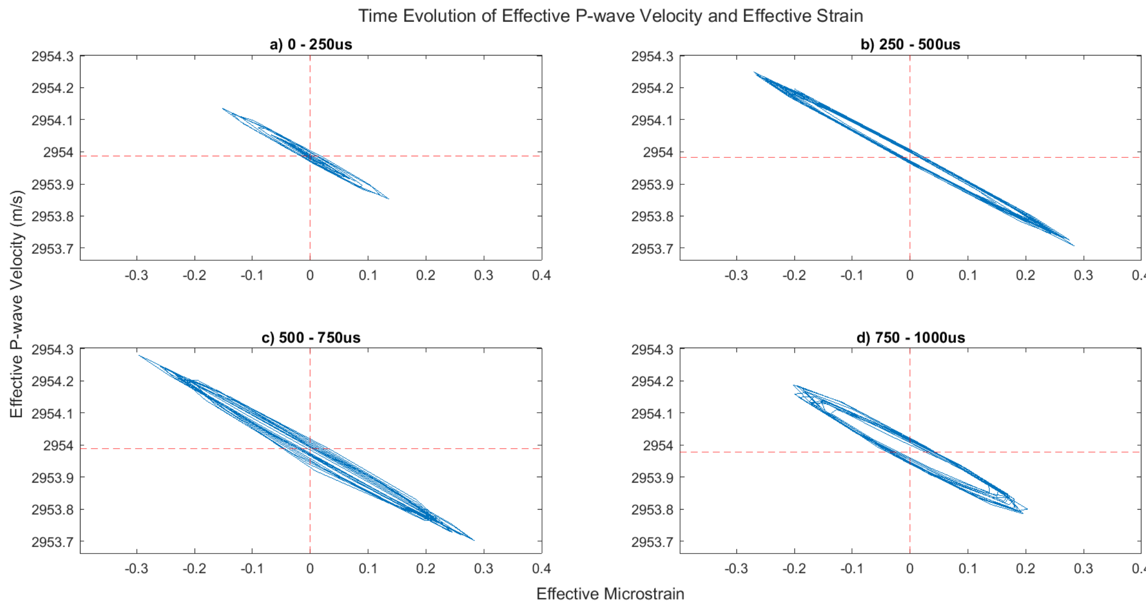

Figure 3.6: The interaction effective velocity for 50 cycles of the pump as a function of the effective strain component ϵ_{33}, in units of microstrain or μm/m. The data are split over four plots, all representing 250μs of the total simulation time of 1000μs in the order (a), (b), (c), (d). The horizontal dashed line marks the mean velocity, and the vertical dashed line marks zero strain. The data in all four plots are traced out counterclockwise.

figure and the data shown in detail.

For clarity, I plot the strain in units of microstrain (μm/m). The effective strain itself is a tensor, and I am interested in the component ϵ_{33}. This is the effective strain acting in the z-direction on a plane parallel to the probe source. More simply, it is the average strain acting normal to the plane containing the crack. For convenience, I write effective strain to mean this component of the strain specifically. My plots show how the effective velocity relates to the effective strain, both measured along the z-direction, as the simulation progresses.

In order to better understand the data in this figure, it is split over four subplots, each representing a quarter of the total simulation time. What is exhibited is well-defined hysteretic behaviour. $v_{interaction}$ can both increase and decrease as the effective strain increases or decreases, giving shape to hysteresis loops. In all four subplots of Figure 3.6, these loops have a fairly constant length and orientation relative to the axis of mean effective velocity. The maximum and minimum $v_{interaction}$ occur at the minimum and maximum effective strains respectively.

Starting with Figure 3.6.a, the loop is fairly short, and the width of each loop appears to be increasing in time. A range of 0.29 microstrains is covered. This indicates a steady state has not yet been attained in the medium.

In Figure 3.6.b, the length of the loop has increased significantly, covering a range of 0.55 microstrains. The width of the loops does not change much, with the same path being traced out repeatedly in time. This indicates that the medium is in a temporary steady state.

Throughout Figure 3.6.c, the loop continues lengthening slightly to a range of 0.58 microstrains. The width of the loop increases in time on average, but not uniformly. The behaviour appears to be moving slightly away from a steady state.

Finally, Figure 3.6.d shows that the loop length decreases to 0.4 microstrains, and is still relatively wide compared to the first 500μs. A steady state has been reached for intermediate strains, but $v_{interaction}$ still varies at the maximum and minimum effective strains.

3.5.2 Effect of Crack on Hysteresis Loops

I propose an explanation for the behaviour of the hysteresis loops between $v_{interaction}$ and the effective strain. Cracks and fracture networks are accepted to be one of the main sources of nonlinearity in rocks. One reason for this is that cracks may open or close with changing strain and changing strain rates including from waves traveling through the cracks. It has been seen that the opening and closing of a crack can cause a change in velocity of waves as they travel through the crack [5]. This phenomenon may also contribute to the existence of hysteretic behaviour between the strain and relative change in velocity as in Rivière [4], or between the strain and velocity as in my data from Figure 3.6.

Haupert et al [2] provide useful observations, with Figure 3.7 taken with permission from their paper for clarity. They look at an aluminum bar with a crack, caused by fatigue damage due to a notch on its edge, running through it. They apply a strain to the sample and measure the relative change in wave speed at three locations in the sample. Two positions are along the crack, and the third is away from the crack. Haupert found that for the position away from the crack, the velocity underwent

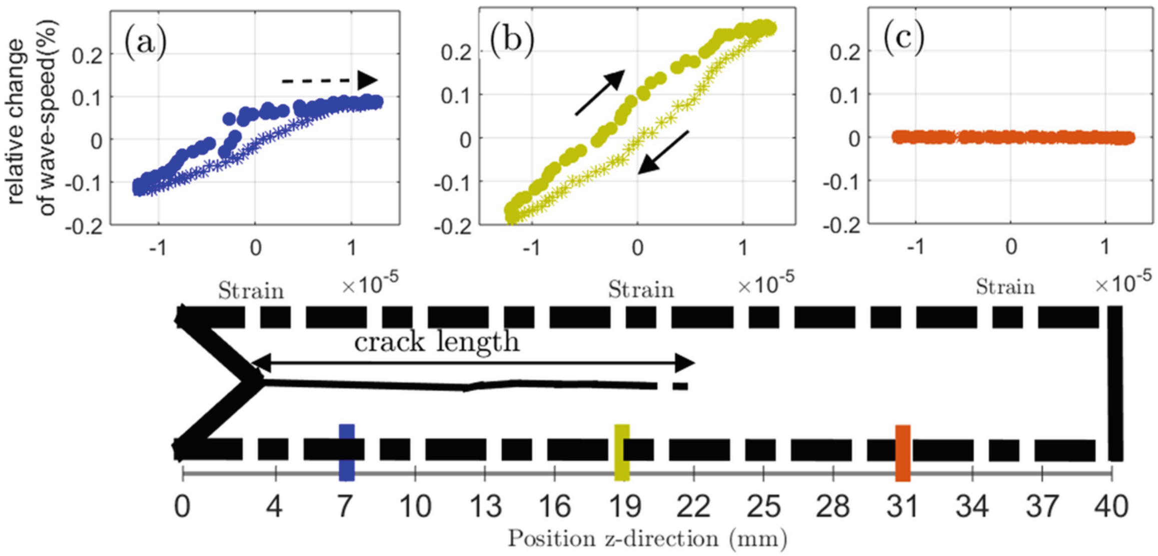

Figure 3.7: Data collected by Haupert, taken from [2]. They measure dynamic responses at three positions in an aluminum bar, with fatigue damage from a notch in the edge of the bar causing a crack, under an applied strain. (a) plots the data for a position at a notch from which the crack extends. (b) is a position at the crack tip, and (c) is a position outside of the crack. All three subplots display hysteretic behaviour between the strain and the relative change in wave speed. The diagram below the plots represents the sample and crack, with the three coloured bars showing the exact positions used in the plots.
Reprinted by permission from Springer Nature: Dynamic Acousto-Elastic Testing by Haupert et al. © Springer International Publishing AG (2019)

very little change as the strain varied, represented by a horizontal line or thin loop on their hysteresis figure. For the two positions along the crack, Haupert found that there was hysteresis in the form of loops, traced out clockwise with increasing strain corresponding to increasing change in relative velocity. Their loops are tilted counterclockwise away from the axis of mean velocity, with the maximum increase in relative velocity occurring at the maximum strain.

I suggest that these observations match my data. The hysteresis loop in Figure 3.7.b, near the edge of Haupert's crack, appears to be very similar to what we observe in Figure 3.6. The main difference is that for Haupert, the maximum change in wave-speed occurs for the maximum positive strain, whereas for my data the maximum $v_{interaction}$ occurs for the maximum negative strain.

This implies that for each time range shown in Figure 3.6, we can apply the

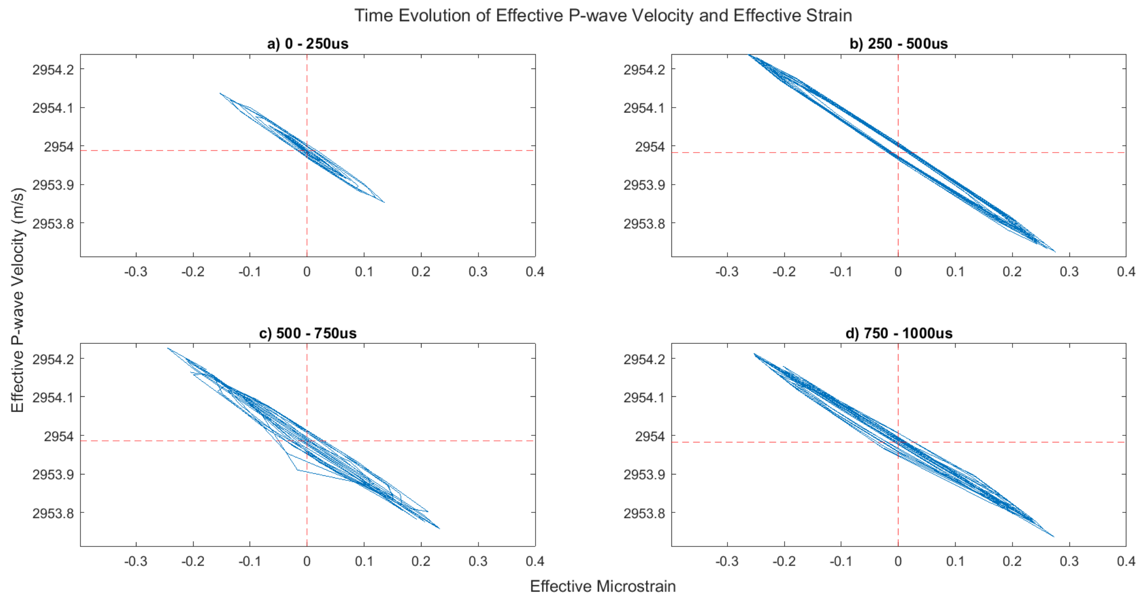

Figure 3.8: The interaction effective velocity for 20 cycles of the pump as a function of the effective strain component ϵ_{33}, in units of microstrain. The data are split over four plots, all representing 250μs of the total simulation time of 1000μs in the order (a), (b), (c), (d). The horizontal dashed line marks the mean velocity, and the vertical dashed line marks zero strain. The data in all four plots are traced out counterclockwise.

explanation provided by Haupert. In particular, I propose that this hysteresis between $v_{interaction}$ and the effective strain arises from the pump and probe waves interacting with the crack. The fact that the maximum effective velocity here corresponds to the maximum magnitude of the effective strain is consistent with previous research by Rusmanugroho [5], which shows that opening and closing of cracks causes these hysteresis loops, and that the opening or closing should be at a maximum for the maximum strain or magnitude.

3.5.3 Observations for 3 and 20 Cycles

As shown in Figure 3.8, plotting $v_{interaction}$ and the effective strain for 20 cycles does show hysteresis behaviour, following very closely to the 50 cycle case in Figure 3.6. Due to the similarity, I discuss the data shown in the figure as a whole, and do not talk individually about the four subplots. The loops do have slightly less uniform behaviour, but the shape, orientation, and range of effective strain are nevertheless approximately the same as for 50 cycles. I believe that the crack is causing the

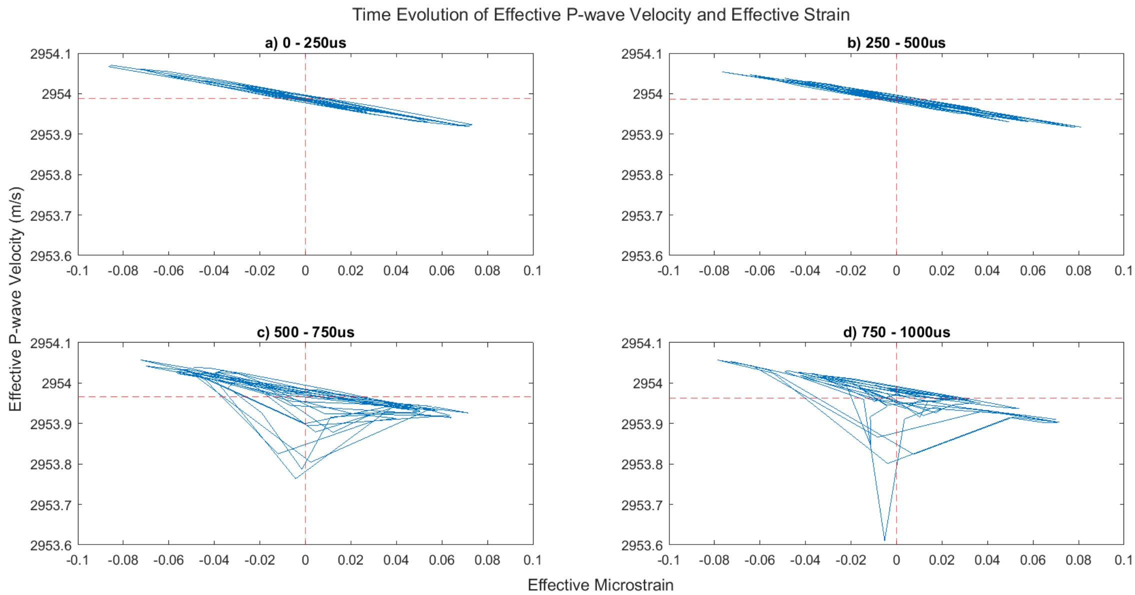

Figure 3.9: The interaction effective velocity for 3 cycles of the pump as a function of the effective strain component ϵ_{33}, in units of microstrain. The data are split over four plots, all representing 250μs of the total simulation time of 1000μs in the order (a), (b), (c), (d). The horizontal dashed line marks the mean velocity, and the vertical dashed line marks zero strain. The data in all four plots are traced out counterclockwise.

hysteresis in this case as well.

The hysteresis for the 3 cycle case, shown in Figure 3.9, is initially similar to that for the 50 cycle case. In Figures 3.9.a and 3.9.b, there is again hysteretic behaviour between $v_{interaction}$ and the effective strain. However, the loops are far less uniform than in the prior cases, with length and width of the loops varying within a brief time frame. In Figures 3.9.c and 3.9.d, the hysteresis has mostly disappeared with noise and many drops in the effective velocity. It seems that while the crack initially interacts with the pump and probe waves, that interaction decreases with time. I believe this indicates that the pump wave interacts with the crack much more strongly than the probe wave does.

Chapter 4

Discussion

4.1 Summary of Steady State Data

I summarize the data for 50 cycles of the pump source as a whole, using a transmission delay of 4μs for the probe source, and in geometry 1 as in Figure 2.1, and give a description and explanation of how the relevant parameters evolve throughout the simulation.

The pump begins broadcasting slightly before the probe, with the waves initially interacting with each other but not with the crack. This interaction leads to a relatively strong nonlinear response, with a steadily growing maximum $v_{interaction}$ amplitude, with this effective wave having a frequency equal to that of the pump wave as seen in an FFT of the velocity, shown in Figure 3.3.c. The growth is due to the interacting waves, and their reflections off the boundaries, creating changing stress and strain fields within the medium. In comparison, when only the probe wave is operating, there is a relatively weak nonlinear response with no clear oscillations in the $v_{control}$, and a small maximum amplitude. The sharp drops in $v_{control}$ seen in Figure 3.1 are likely numerical artifacts due to the method of averaging over a representative volume. This indicates that the stress and strain fields induced by the probe are much smaller than those induced by the pump, as expected due to the amplitude of the pump source being 100 times that of the probe source.

As discussed in the prior section, we see a hysteresis loop between the $v_{interaction}$ and the effective strain, which grows and shrinks slightly in length as the simulation time progresses. This arises from the pump wave interacting with the crack and causing it to open and close, in turn perturbing the probe and pump waves. It is not entirely clear what causes the loops to lengthen and compress. However, these time frames do correspond to $v_{interaction}$ increasing and decreasing in amplitude respectively, and as discussed before, this is influenced by the reflections of the source waves off the boundaries.

In general, while $v_{interaction}$ does increase and then decrease as the simulation progresses, it remains at a somewhat smooth, non-oscillatory maximum amplitude, with no large shifts due to the crack, and roughly resembles a steady state.

Figure 3.5.c illustrates the time delay for 50 cycles of the pump. Throughout the upper half of the model, along the range of $z = 0$ m to $z = 0.85$ m, the time delay between $v_{interaction}$ and $v_{control}$ begins to increase, with the control effective wave having a slightly higher velocity. As discussed previously, there is a large drop in time delay around $z = 0.85$ m, after which the time delay is negative. Based on the location at which this occurs, it is likely that the drop is due to the probe wave passing out of the region of influence of the pump wave, leading to an increase in $v_{interaction}$ in this region. Note that the crack does not appear to have a noticeable effect on the time delay.

4.2 Summary of Transient States

I briefly compare my steady state approximation of resonance with 50 cycles to the non-resonance conditions of 20 cycles and 3 cycles. The important aspect, as mentioned in brief before, is that there is a fairly continuous, albeit gradual, transition between them.

Taken as a whole, we see that the simulation for 20 cycles is comparable to the simulation for 50 cycles. While the specific behaviour and trends do not match completely, the evolution of the stress and strains in the medium occur similarly. Either case is sufficient to exhibit hysteresis between $v_{interaction}$ and the effective strain by perturbing the crack; to cause an increase in that velocity as it passes out of the pump wave; and for the effective velocity to oscillate at the pump frequency. For the simulation time and model geometry used, we do not need to be perfectly at a steady state to observe this behaviour.

The steady state case and the transient case of 3 cycles display very different behaviour. The appearance of hysteresis and the opening and closing of the crack; the oscillatory $v_{interaction}$ with a defined underlying frequency; and the decreasing time delay do not occur in this case, being dependent on the time for which the pump is broadcast. Using this model, we cannot describe the same behaviour through both the transient and steady state cases.

4.3 Comparison to Literature

4.3.1 DAET

I begin by comparing my steady state results to data found with resonance DAET. As I have discussed before, the hysteresis we observe between the effective strain and $v_{interaction}$ matches with that seen by Haupert and shown in Figure 3.7. In particular, their explanation that the crack is responsible for the hysteresis seems valid here as well. This relation between the strain and relative velocity is a common observation in DAET experiments, and not seen in non-resonant DAET. Haupert also notes that the orientation of the loops in Figure 3.6, with higher effective velocities occurring when the effective strain is negative than when it is positive, has also been observed experimentally in samples of granite.

Haupert [2] further discusses the main underlying frequency of the effective velocity being the pump frequency, which we observe in Figure 3.3. They also observe a second frequency near zero, which is not evident in my steady state data, but is actually present in my transient data. There is not enough evidence to say if this peak is relevant, or simply coincidental.

As in Rivière [4], the simulation requires a fairly long period before the effective velocity reaches resonance, where changes in the amplitude are small, albeit less uniformly in my data.

I make one final note. Renaud [3] plots the time delay for various samples in terms of the pump pressure, presented in a different form than my time delay data. They are not directly comparable, but the data taken by Renaud does show that the time delay may be both positive and negative at different regions, as we have seen in Figure 3.5. This suggests that the negative time delays may arise from the actual dynamics in our medium, and not simply some numerical artifact.

As a whole, it is difficult to tell from my existing data if my model at steady state can accurately represent all of the experimental results found with DAET. The work of Rivière in particular is more in-depth and detailed than what is done with this model. Further, few papers present the effective velocity as a function of simulation time, choosing instead the pressure or stress and making comparisons more complicated to perform. The model I use is much less complex than experimental samples. However, we still see some major similarities to existing research, in particular the presence of hysteresis loops between $v_{interaction}$ and the effective strain, and the explanation matches our observations. Therefore I believe that this numerical model can be used as a valid, albeit very simple, application of DAET.

4.3.2 Non-Resonant DAET

I now compare my transient results to data found with non-resonant DAET. Gallot [1] notes that when using only a few cycles of the pump wave, the probe wave does not cause sufficient interactions to observe hysteresis, as we have seen. They also find that the main source of the strain within the sample is the pump wave. My data shows similar behaviour as in Figure 3.2, where $v_{interaction}$ for 3 pump cycles has a much smaller amplitude and less uniform shape compared to the other two simulations, where the pump plays a larger role.

When modeling time delay, TenCate [9] showed that the mean of the time delay increases as the pump wave interacts more with the probe wave, and that the oscillations in the time delay are related to the pump frequency. While this does not exactly match my data for 3 cycles, this may account for the increasing time delay. As the pump only broadcasts briefly, the amplitude and frequency of the pump wave traveling in the medium may be disrupted more from their original sinusoidal form, causing reflections to occur at varying phases instead of a more confined phase shift when the pump broadcasts for longer. I note that for our data, the oscillations in the time delay are actually slightly less than twice the frequency of the probe wave, not the pump wave. Though not directly calculated there, the oscillations are shown in Figure 3.5. This seems reasonable at the boundaries of the medium far from the crack and pump source, as the pump is oriented to broadcast perpendicular to the z-axis, and so we expect to see the effects due to the pump decrease towards the boundaries with the probe wave having more influence on the $v_{interaction}$, especially when the pump is only broadcast for 3 cycles.

Rusmanugroho [5] has used a previous version of this model to study the effects of cracks on nonlinear wave interactions. I briefly point out that their plot for time delay across the z-axis of the medium is fairly similar in form to the one we see now, which is expected. They do not see oscillations or a negative time delay, but they do see the drop in time delay around the midpoint of the model as we observed, followed by a rapid increase. However, Rusmanugroho suggests that the drop in time delay is due to the pump wave opening and closing the cracks in their medium, and that the subsequent increasing time delay is due to the pump wave holding the cracks open and the probe wave then travelling through those open cracks. While this is a possible explanation for why the time delay increases significantly in my transient case, I do not think it accounts for the drop and still consider the cause to be the effective wave passing out of the region of influence of the pump.

It is unsurprising that these results do not completely match those from the experiments of Gallot and TenCate. My numerical medium is considerably simpler than the rock they examine, only having a single crack instead of many possible fracture networks; does not have exactly the same dimensions as their sample, although I demonstrated that the differences should have fairly small qualitative effect; and is idealized with well-defined background parameters. However, we do see enough similarities for my model to be applicable to this method.

Chapter 5

Conclusions and Looking Forward

5.1 Future Work

The results of my work suggest many possible directions for future work. The most logical next step would be to increase the number of cracks in the medium, perhaps randomly distributed, in order to better approximate a real rock sample, which has many cracks or fracture networks. It would be interesting to determine if the behaviour we see here, with the hysteresis loops, the drop in time delay, and the smooth change in maximum amplitude for $v_{interaction}$, would be preserved or significantly changed in this scenario. Another simple test would be to significantly increase the total simulation time while still using 50 pump cycles, to see if $v_{interaction}$ does eventually decay back to some mean after the pump stops broadcasting.

There are also two areas that I looked into briefly during my work for this thesis that I have decided are not currently relevant, but certainly exhibit interesting behaviour for future work. The first is changing the geometry of the model, particularly when doubling the length along the z-axis. As shown in Figure 3.4, this new geometry causes a major change in $v_{interaction}$ when 50 pump cycles are used. More simulations could be done to determine what exactly causes this large increase in amplitude.

The second area involves hysteresis, but not between the effective strain and the effective velocity. Instead, I have found that there is hysteretic behaviour between the force broadcast by the pump source and the effective velocity. In particular, the hysteresis loops begin to rotate in time. This is not mentioned in the literature for DAET, and thus is not within the purview of my thesis. Nevertheless it is an interesting observation, and it may be worth determining if it is a numerical effect or more meaningful.

5.2 Final Notes

I have used a finite difference scheme to model the interactions of a pump wave and a probe wave within a cracked, nonlinear medium. By varying the number of cycles for which the pump is broadcast, I obtained data for the two cases of a resonant state approximated by a steady state, and for a transient state. My main results are shown and discussed in terms of the effective velocity; a delay in travel time between the case with a probe with no pump and the case with both probe and pump; and hysteretic behaviour between the effective velocity and the effective strain. In particular, I found that the resonant and transient cases do display notably different behaviour. Using this model, we cannot describe the same behaviour through both the transient and steady state cases.

These findings were then compared to experimental data using either Dynamic Acousto-Elastic Testing (DAET) or modified non-resonant DAET. I discussed numerous similarities between my data and those from the literature, and found that some of the major aspects of each method and state are exhibited in my simulations. There were differences as well, which may be accounted for by the simplicity of the model relative to experimental samples. While more simulations may be helpful, I have proposed that the model as a whole is applicable to both resonant DAET and non-resonant DAET using the resonant state and the transient state respectively.

Bibliography

[1] T. Gallot, A. E. Malcolm, T. L. .Szabo, S. Brown, D. Burns, and M. Fehler. Characterizing the nonlinear interaction of S- and P-waves in a rock sample. *Journal of Applied Physics*, 117, 2015.

[2] S. Haupert, G. Renaud, J. Rivière, and P. Shokouhi. Dynamic acouto-elastic testing. In *Nonlinear Ultrasonic and Vibro-Acoustical Techniques for Nondestructive Evaluation*. Springer International Publishing, 2019.

[3] G. Renaud, S. Callé, and M. Defontaine. Remote dynamic acoustoelastic testing: Elastic and dissipative acoustic nonlinearities measured under hydrostatic tension and compression. *Applied Physics Letters*, 94, 2009.

[4] J. Rivière, G. Renaud, R. A. Guyer, and P. A. Johnson. Pump and probe waves in dynamic acousto-elasticity: Comprehensive description and comparison with nonlinear elastic theories. *Journal of Applied Physics*, 114(5), 2013.

[5] H. Rusmanugroho, A. Malcolm, and M. Darijani. A numerical model for the nonlinear interaction of elastic waves with cracks. *Wave Motion*, 92, 2020.

[6] M. Schoenberg. Elastic wave behavior across linear slip interfaces. *Journal of the Acoustical Society of America*, 68(5), 1980.

[7] M. Schoenberg and C. M. Sayers. Seismic anisotropy of fractured rock. *Geophysics*, 60(1), 1995.

[8] J. A. TenCate. Slow dynamics of earth materials: An experimental overview. *Pure and Applied Geophysics*, 168, 2011.

[9] J. A. TenCate, A. E. Malcolm, X. Feng, and M. C. Fehler. The effect of crack orientation on the nonlinear interaction of a P wave with an S wave. *Geophysical Research Letters*, 43(12), 2016.